RSC Advances

PAPER

View Article Online
View Journal | View Issue

Cite this: *RSC Adv.*, 2019, **9**, 10999

Enhanced up-conversion luminescence in transparent glass-ceramic containing $KEr_3F_{10}:Er^{3+}$ nanocrystals and its application in temperature detection

Zhijun Xia,[a] Huixiang Huang,[a] Zhi Chen,[a] Zaijin Fang[c] and Jianrong Qiu *[ab]

Received 14th March 2019
Accepted 2nd April 2019

DOI: 10.1039/c9ra01945f

rsc.li/rsc-advances

Transparent Er^{3+} doped glass-ceramics containing $KEr_3F_{10}:Er^{3+}$ nanocrystals were prepared *via* the traditional melt-quenching technique. The micro-structures, optical properties and up-conversion luminescence behaviors of the Er^{3+} doped glass-ceramics were systemically studied using X-ray diffraction, absorption and up-conversion luminescence spectra. Under the excitation of a laser at 980 nm, the intensity of red emission of the glass-ceramics increases more than 70 times after heat treatment compared with that of the precursor glass ceramic. Moreover, the fluorescence intensity ratio of the thermally coupled energy levels ($^2H_{11/2}$ and $^4S_{3/2}$) shows a good linear relationship with temperature and maintains relatively high sensitivities of 0.398% per K at 303–573 K, which indicates that the glass ceramics have promising applications in temperature detection.

Introduction

In recent years, rare earth (RE) ion doped up-conversion materials, including nanoparticles, glasses and glass-ceramics, have attracted wide attention because of their excellent characteristics and potential application prospects in solid-state lasers, multi-color displays, optical processing sensors, solar cells, bio-imaging *etc.*[1–8]

Compared with traditional oxyfluoride glass, RE doped transparent fluoride glass-ceramics have excellent optical properties and mechanical properties. They have a higher refractive index, lower local phonon energy and lower non-radiative relaxation probability, so high luminescence efficiency of REs has been observed.[9,10] In view of this, a large number of oxyfluoride glass-ceramics have been studied and considered as excellent hosts for rare earth ions to realize efficient up-conversion luminescence.[11–19] In these systems, the doping ions usually enter the crystalline lattice mainly through the diffusion of rare earth ions from the glass matrix to the precipitated crystals, which is greatly affected by the diffusion activation energy and diffusion coefficient of the RE ions in the glass.[20] Usually, at lower crystallization temperatures, the low diffusion coefficient of rare earth ions in the glass hinders their bonding in the crystal, while at high crystallization temperatures, the rapid growth of the grains significantly reduces the transparency of the glass-ceramics, thus resulting in unfavorable optical performance. Therefore, it is meaningful to prepare oxyfluoride glass-ceramics with good stability and transparency.

Among many rare earth ions, Er^{3+} ions is considered as the most ideal rare earth ions for near-infrared up-conversion due to its rich 4f–4f transition level. Moreover, Er^{3+} ions have a couple of thermally coupled energy levels (TCEL), $^2H_{11/2}$ and $^4S_{3/2}$ levels. Therefore, application of Er^{3+} doped glass-ceramics as optical temperature sensors has attracted increasing attention in recent years.[21–24] What's more, there is no report on optical temperature measurement of Er^{3+} doped KEr_3F_{10} glass-ceramics. Therefore, it is of great significance to study the up-conversion luminescence and temperature sensing properties of Er^{3+} doped KEr_3F_{10} glass-ceramics.

In this paper, highly transparent glass-ceramics containing KEr_3F_{10} nanoparticles were successfully fabricated by properly designing the oxyfluoride glass composition. Unlike previously reported cases, glass-ceramics are formed directly by self-crystallization during melt quenching, and Er^{3+} is directly incorporated into the crystalline lattice rather than entering the already formed lattice during heat treatment. After heat treatment, the luminescence is enhanced more than 70 times. In addition, based on the fluorescence intensity ratio (FIR) technology, the temperature sensing characteristics of the glass-ceramic are also investigated.

[a]*State Key Laboratory of Luminescent Materials and Devices, Institute of Optical Communication Materials, South China University of Technology, Wushan Road 381, Guangzhou 510641, China. E-mail: qjr@scut.edu.cn*

[b]*State Key Laboratory of Modern Optical Instrumentation, College of Optical Science and Engineering, Zhejiang University, Hangzhou 310027, China*

[c]*Guangdong Provincial Key Laboratory of Optical Fiber Sensing and Communications, Institute of Photonics Technology, Jinan University, Guangzhou 510632, China*

Experiment

Precursor samples were prepared by melt-quenching method. The precursor glass (PG) compositions (mol%) is 22.5 KF-22.5 ZnF_2-65 SiO_2, ErF_3 (0.1, 0.3, 0.5, 1, 1.5, 3 mol%). SiO_2 (99.9%), ZnF (99.9%), KF (99.5%) and ErF_3 (99.99%) were used as raw materials. About

20 g of a mixture of raw materials was placed into a covered platinum crucible and melted at 1450 °C for 30 minutes. Then, the glass melt was poured onto a 300 °C preheated stainless-steel plate and pressed by another plate to obtain the PG samples. After releasing the internal stress by heating at 450 °C for 3 h, the PG samples were crystallized by heat-treatment at 625 °C for 10 h to fabricate transparent glass ceramic (GC). All of the samples were polished carefully prior to optical measurements.

X-ray diffraction (XRD) patterns were acquired using a Philips X′ Pert PRO SUPER X-ray diffractometer (40 kV, 40 mA) equipped with a Cu Kα radiation source. The absorption spectra of the glass-ceramic samples were measured by a UV-Vis-NIR spectrophotometer Lambda 900 (PerkinElmer, USA). The morphology and crystal size of the nanocrystals in GC were obtained by high-resolution transmission electron microscope (HRTEM, 2100F, JEOL, Japan) The emission spectra of the samples were obtained using a computer Triax 320 type spectrometer (Jobin-Yvon Corp.) with a 980 nm continuous-wave laser. The pump power was adjusted through neutral density filters. The temperature-dependent spectra of the samples in the range of 298 to 573 K were also measured by the above spectrometers equipped with a temperature controller (FOTEK MT48-V-E, Taiwan). Except for the temperature dependent upconversion luminescence spectra, all of the above tests were performed at room temperature.

Results and discussion

Fig. 1(a) shows the XRD patterns of different concentration Er^{3+} doped samples. PG shows weak diffraction peaks when the Er^{3+} doping concentration reaches 0.5%. The diffusion peak is caused by the amorphous glass phase, while the weak diffraction peaks means that a small amount of nanocrystals have formed after melt-quenching. XRD patterns of PG and GC are shown in Fig. 1(b). After heat treatment at 625 °C for 10 h, the diffraction peaks of GC sample corresponding to KEr_3F_{10} nanocrystals (PDF no. 26-1311) become intense, which indicates that more nanocrystals are formed after the heat treatment. TEM images of GC sample are shown in Fig. 1(c). TEM micrograph reveals that KEr_3F_{10} nanocrystals are homogeneously dispersed in amorphous glassy phase. The corresponding selected area electron diffraction (SAED) patterns indicate that glass-ceramics are composite materials that contain amorphous glasses and nanocrystals. The HRTEM image shows the resolved lattice fringes and the value of the associated interplanar spacing d is about 0.463 nm, which corresponds to (−2 0 7) crystal plane of KEr_3F_{10} (d = 0.462 nm).

Fig. 2(a) shows the upconversion spectra of PG and GC samples doped with 1% (mol) Er^{3+} excited by 980 nm laser. The emission bands located at 523 nm, 543 nm and 665 nm are assigned to $^2H_{11/2} \rightarrow {}^4I_{15/2}$, $^4S_{3/2} \rightarrow {}^4I_{15/2}$ and $^4F_{9/2} \rightarrow {}^4I_{15/2}$ transition emissions of Er^{3+}, severally.[25,26] It is clear that the upconversion spectra of the sample show obvious Stark splitting at 543 and 665 nm. After heat treatment, the upconversion intensity of GC is greatly enhanced; although a few Er^{3+} ions have already participated into KEr_3F_{10} nanocrystals before heat treatment. Specifically, the upconversion intensity of red emission of the GC enhances by more than 70 times compared to that of the PG. The enhance of upconversion luminescence may be due to the incorporation of Er^{3+} ions into KEr_3F_{10}

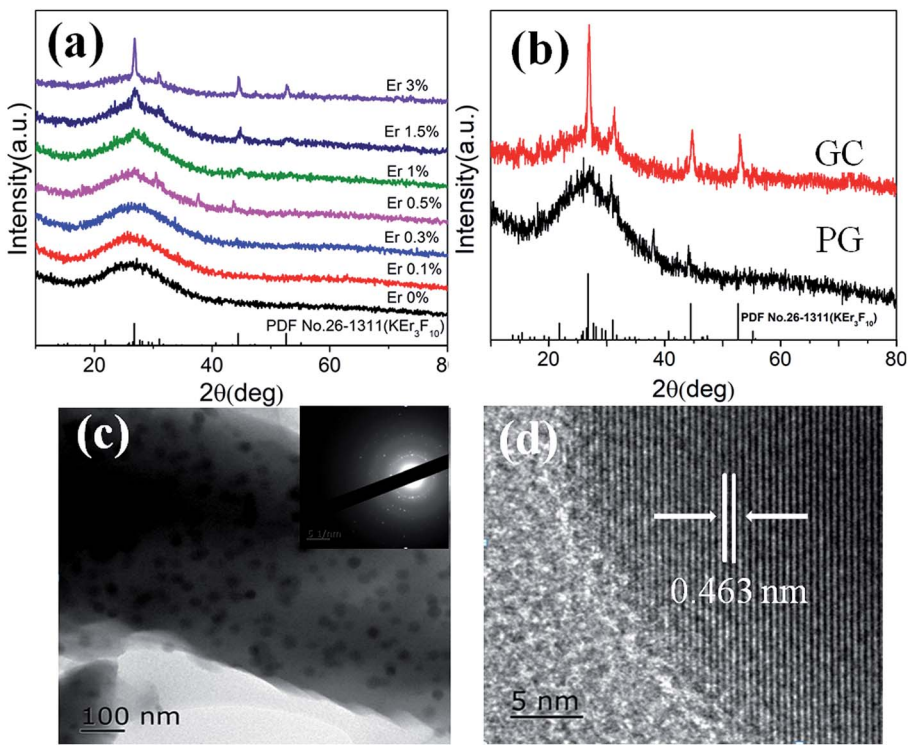

Fig. 1 (a) XRD patterns of different concentration Er^{3+} doped glass samples; (b) XRD pattern of PG, GC samples and standard XRD data of PDF card no. 26-1311 for KEr_3F_{10}; (c) TEM micrograph of GC and corresponding SAED pattern. (d) HRTEM image of GC.

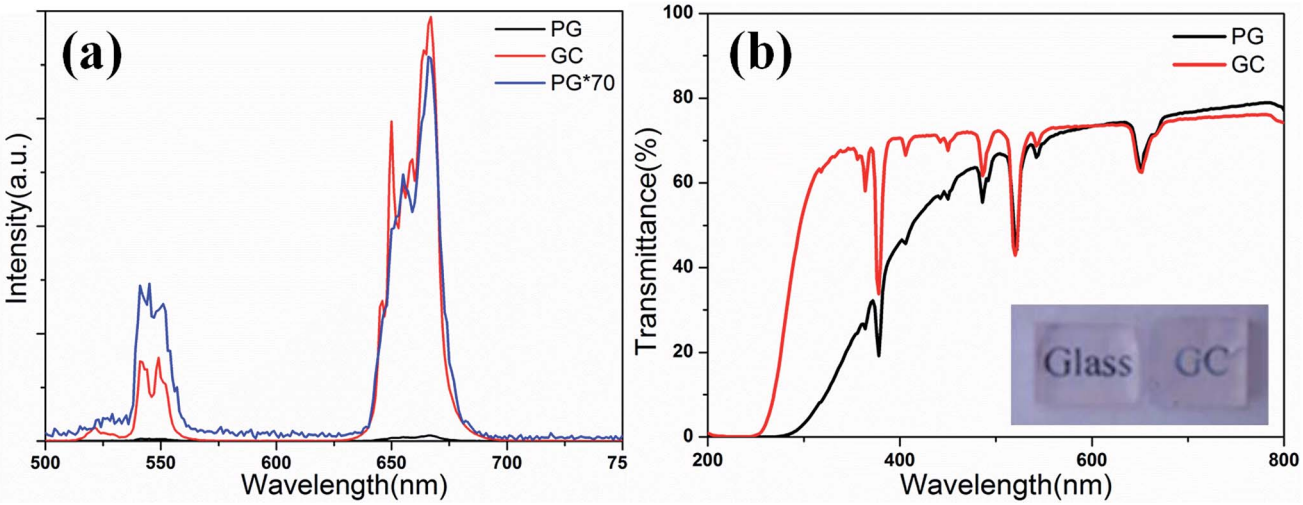

Fig. 2 (a) Upconversion spectra of PG and GC samples excited by 980 nm laser; (b) transmission spectra of PG and GC samples and the inset is the photograph of PG and GC.

nanocrystals with lower phonon energy and the enrichment of Er^{3+} resulting in the change of the energy transfer mode between Er^{3+}. From the transmission spectra of PG and GC samples shown in Fig. 2(b), it can be observed that PG and GC maintain good transparency and the transparency of GC is up to 76% in visible region. It can be seen that KEr_3F_{10} glass-ceramics are transparent with excellent uniformity, indicative of homogeneous crystallization of these samples.

For the upconversion process, upconversion emission intensity I is proportional to the nth power of the pump power P, that is[27]

$$I \propto P^n \quad (1)$$

where n is the number of pump photons absorbed per upconversion photon emitted. A plot of $\log I$ *versus* $\log P$ yields a straight line with slope n. Fig. 3(a) and (b) show the power dependences of upconversion of PG and GC samples, respectively. For PG, the slopes n values are 1.81 ± 0.03 and 1.69 ± 0.03 for green and red emission, respectively. As to GC, n values are 1.79 ± 0.03 and 1.73 ± 0.03. The results reveal that both red and green upconversion emissions are caused by two-photon process.

Fig. 4(a) shows the fluorescent lifetime curves of Er^{3+} $^4F_{9/2} \rightarrow {}^4I_{15/2}$ (666 nm) emission in PG and GC samples upon 980 nm LD. The prolongation of upconversion emission lifetime shows that the non-radiative relaxation rate of Er^{3+} in the GC sample decreases, which proves that Er^{3+} ions are preferentially enriched in KEr_3F_{10} nanocrystals with lower phonon energy. The fluorescent lifetime curve of GC can be well fitted with a double exponential unction, which indicates that GC samples have multi-luminescent centers.

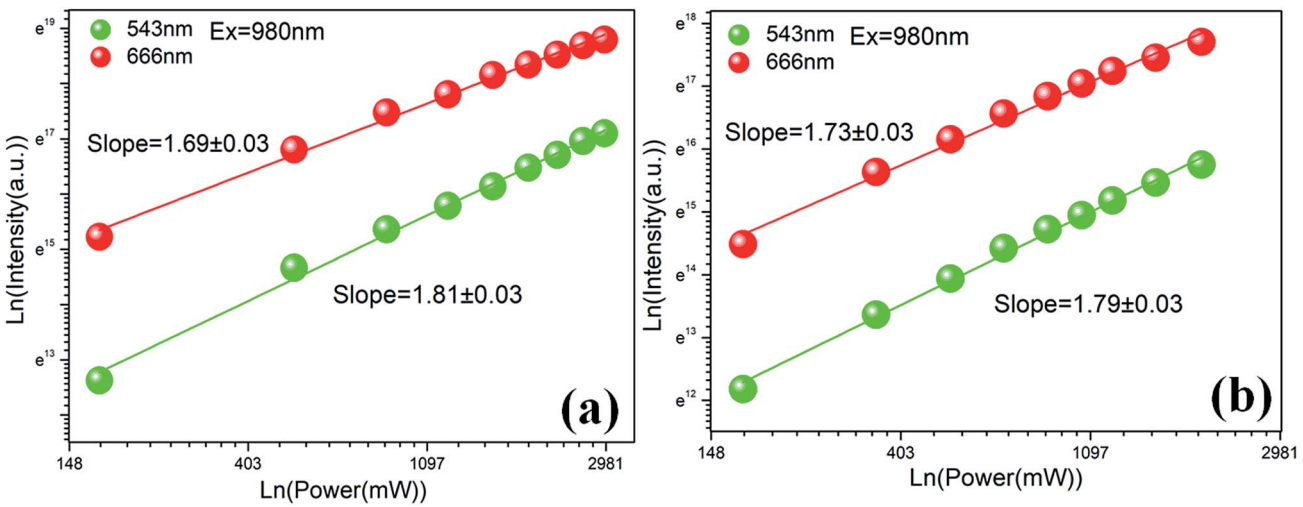

Fig. 3 (a) Dependence of upconversion intensity on pump power for PG sample; (b) dependence of upconversion intensity on pump power for GC sample.

To understand the upconversion mechanism, the energy level diagram of Er^{3+} and possible upconversion mechanisms are shown in Fig. 4(b). Firstly, Er^{3+} ions in the ground state of $^4I_{15/2}$ absorb a 980 nm phonon and be pumped to the intermediate excited state of $^4I_{11/2}$ through ground state absorption (GSA). Then, these ions at $^4I_{11/2}$ level can be excited to higher emitting levels through two famous upconversion processes: (1) excited state absorption (ESA), (2) energy transfer (ET). ESA process is a single ion process. The ET process involves two ions and therefore the rate depends largely on the distance between the active ions.

Because only a bit of KEr_3F_{10}:Er^{3+}nanocrystals form in PG, a small amount of Er^{3+} ions merge into KEr_3F_{10}:Er^{3+} nanocrystals with low phonon energy and most of Er^{3+} are persisted in the glass phase, which can be confirmed by the weak stark splitting in PG (see Fig. 2(a)). ET and ESA process are responsible for the $^2H_{11/2}$, $^4S_{3/2}$ and $^4F_{9/2}$ emission levels. ESA maybe the dominant process due to the uniform dispersion of Er^{3+} ions in the glass and the relatively long distance between Er^{3+} ions.

By absorbing one 980 nm photon, Er^{3+} ions at $^4I_{11/2}$ level are stimulated to the level of $^4F_{7/2}$ by ESA process, and then non-radiatively relax to the level of $^2H_{11/2}$ and $^4S_{3/2}$ levels. Finally, Er^{3+} ions at $^2H_{11/2}$ and $^4S_{3/2}$ emitting further relax to $^4I_{15/2}$ level and produce upconversion emissions at 525 and 543 nm, respectively. For the red emission, there are two possible ways, including multi-phonon non-radiative relaxation from the upper level of $^4S_{3/2}$ and a ESA processes: Er^{3+} ions absorb another photon from $^4I_{13/2}$ level.[22,27] Intermediate excited states in $^4I_{13/2}$ can be filled by multi-phonon non-radiation processes at $^4I_{11/2}$ level and high radiation processes at $^4S_{3/2}$ level.[18] Finally, the Er^{3+} ions radiation at $^4F_{9/2}$ level relaxes to $^4I_{15/2}$ ground state and produce red emission at 666 nm.

For GC sample, since the distance of Er^{3+}–Er^{3+} is further shortened, the up-conversion mechanism belongs to ET process, which is a more efficient way for Er^{3+} ions at $^4I_{11/2}$ level to be excited to higher emitting levels and produce stronger up-conversion luminescence. An excited Er^{3+} ion at $^4I_{11/2}$ level relaxes non-radiatively to $^4I_{15/2}$ level and transfers its excitation energy to a neighboring Er^{3+} ion at the same level, promoting the latter to $^4F_{7/2}$ level: $^4I_{11/2} + {}^4I_{11/2} \rightarrow {}^4I_{15/2} + {}^4F_{7/2}$.[25] The red luminescent $^4F_{9/2}$ level can be excited by the ET process: $^4I_{13/2} + {}^4I_{11/2} \rightarrow {}^4F_{9/2} + {}^4I_{15/2}$.[27] The emission intensity enhancement of red is more than green after further heat treatment, which can be considered as another energy transfer process, $^4F_{7/2} + {}^4I_{15/2} \rightarrow {}^4I_{11/2} + {}^4I_{11/2}$. Since the $^4F_{7/2}$ level plays an important role in the green light emission process, the red emission in Fig. 2(a) is stronger than the green emission.

Fig. 5(a) is normalized upconversion spectra of the GC sample in the temperature range of 303–573 K under a 980 nm LD excitation. It is obvious that the intensity of $^2H_{11/2} \rightarrow {}^4I_{15/2}$ transition (525 nm) and $^4S_{3/2} \rightarrow {}^4I_{15/2}$ transition (543 nm) increases obviously as the temperature raises. Fig. 5(b) shows the temperature dependence of FIR between $^2H_{11/2} \rightarrow {}^4I_{15/2}$ and $^4S_{3/2} \rightarrow {}^4I_{15/2}$ transitions of Er^{3+}. Interestingly, the intensity of Er^{3+} exhibits a significantly different temperature dependent luminescence behavior compare to previous studies.[18,21–24]. The FIR of the TCEL ($^2H_{11/2}$ and $^4S_{3/2}$) shows good linear temperature dependence. From 303 to 573 K the following linear dependence of FIR on temperature is found for KEr_3F_{10}:Er^{3+}:

$$\mathrm{FIR} = -0.93 + 0.00398T \quad (2)$$

It is different from the general temperature sensors that the sensitivity is enhanced first and then weakened. The sensitivity of GC sample maintains a relative high value of 0.398% per K at 303–573 K. This value is larger than most of other Er^{3+} ions doped glass and glass ceramics as listed in Table 1. The fluorescent lifetime curve of the glass ceramic sample can be well fitted with a double exponential function, which indicates that the sample has multi-luminescent centers. For the system with multiple luminescent centers, the number of particles in each excited state varies due to the energy transfer between ions, which may not obey Boltzmann distribution strictly.[28] This result indicates that KEr_3F_{10}:Er^{3+} glass-ceramics is a promising optical temperature sensing.

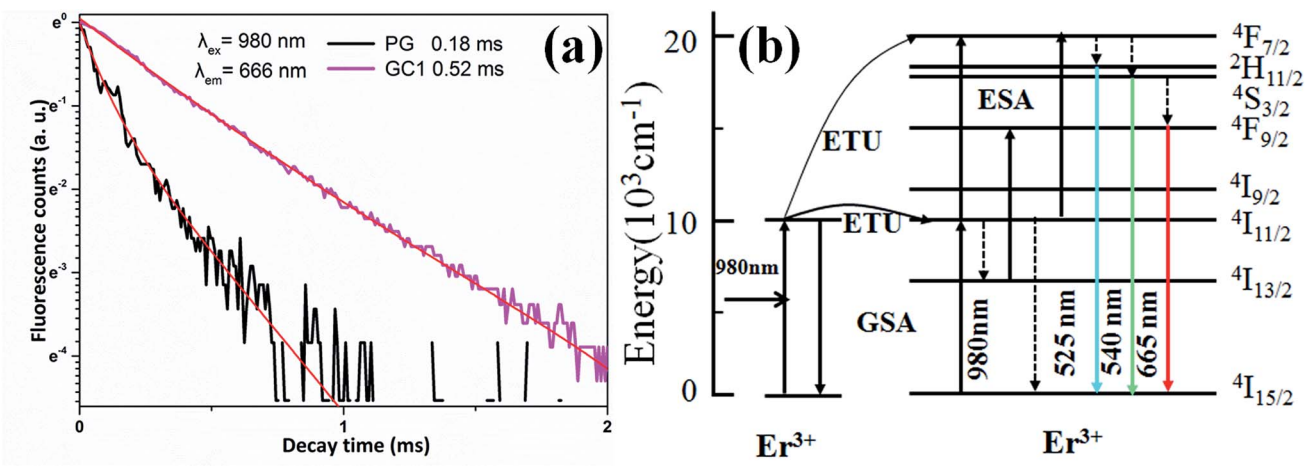

Fig. 4 (a) The fluorescence decay curves of Er^{3+} $^4F_{9/2} \rightarrow {}^4I_{15/2}$ (666 nm) emission in PG and GC samples ($\lambda_{ex} = 980$ nm). (b) Energy level diagram of Er^{3+} and possible up-conversion mechanisms.

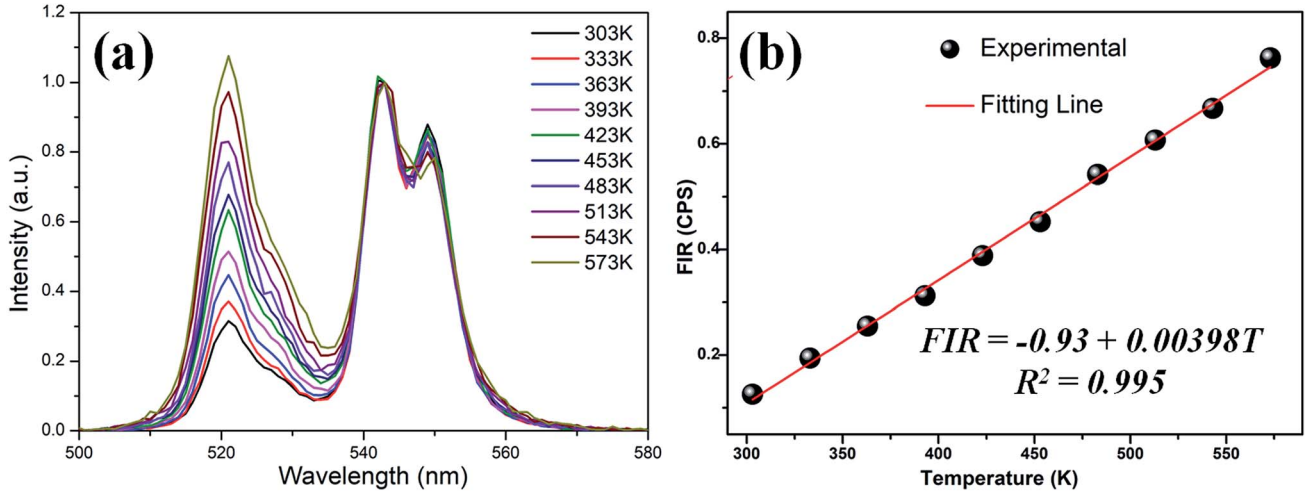

Fig. 5 (a) The normalized green up-conversion spectra of GC sample in the temperature range of 303–573 K under 980 nm LD excitation; (b) temperature dependence of FIR between $^2H_{11/2} \rightarrow {}^4I_{15/2}$ and $^4S_{3/2} \rightarrow {}^4I_{15/2}$ transitions of Er^{3+}.

Table 1 Sensitivity of several optical temperature sensors based on up-conversion emission from $^2H_{11/2}$ and $^4S_{3/2}$ levels of Er^{3+} ion

Sensing materials	Temperature range (K)	S_{max} (10^{-3}/K)	Temperature (K)	Ref.
KEr_3F_{10}:Er^{3+}GC	303–573	3.98	303–573	This work
Sr^2YbF^7:Er^{3+}GC	300–500	6.21	560	21
CaF_2:Er^{3+}glass	303–573	2.38	483	23
CaF_2:Er^{3+}GC	303–573	1.63	453	23
$Na_5Gd_9F_{32}$:Er^{3+}GC	300–510	1.79	499	22
K_3YF_6:Er^{3+}GC	300–510	1.27	300	18
$NaYF_4$:Er^{3+}/Yb^{3+}GC	298–693	0.35	560	24

Conclusion

Er^{3+}-doped transparent KEr_3F_{10} glass-ceramics were prepared *via* the melt-quenching method and subsequent heat treatment process. Significant Stark splitting, enhanced up-conversion emission in glass ceramics and extended fluorescent lifetime indicate that Er^{3+} preferentially enters KEr_3F_{10} nanocrystals with low phonon energy and shorter Er^{3+}–Er^{3+} distance after heat treatment. The FIR of the 525 nm and 543 nm shows good linear dependence and high sensitivity, which suggests that the explored KEr_3F_{10} GC doped with Er^{3+} shows great potential for optical temperature sensing.

Conflicts of interest

There are no conflicts to declare.

Acknowledgements

This work is financially supported by the National Key R&D Program of China (no. 2018YFB1107200), National Natural Science Foundation of China (no. 51772270), Open Funds of State Key Laboratory of Precision Spectroscopy (East China Normal University) and State Key Laboratory of High Field Laser Physics (Shanghai Institute of Optics and Fine Mechanics, Chinese Academy of Sciences), and the Fundamental Research Funds for the Central Universities.

References

1 F. Auzel, *Chem. Rev.*, 2004, **35**, 139–173.
2 F. Wang, Y. Han, C. Lim, Y. Lu, J. Wang, J. Xu, H. Chen, C. Zhang, M. Hong and X. Liu, *Nature*, 2010, **463**, 1061–1065.
3 F. Wang, R. Deng, J. Wang, Q. Wang, Y. Han, H. Zhu, X. Chen and X. Liu, *Nat. Mater.*, 2011, **10**, 968–973.
4 J. Zhou, G. Chen, E. Wu, G. Bi, B. Wu, Y. Teng, S. Zhou and J. Qiu, *Nano Lett.*, 2013, **13**, 2241–2246.
5 H. Lin, G. Meredith, S. Jiang, X. Peng, T. Luo, N. Peyghambarian and Y. B. Pun, *J. Appl. Phys.*, 2003, **93**, 186–191.
6 Z. Chen, W. Cui, S. Kang, H. Zhang, G. Dong, C. Jiang, S. Zhou and J. Qiu, *Adv. Opt. Mater.*, 2017, **5**, 1600554.
7 Z. Chen, H. Jia, X. Zhang, J. Liu, S. Zeng, Y. Li, Z. Ma, G. Dong and J. Qiu, *J. Am. Ceram. Soc.*, 2015, **98**, 2508–2513.
8 E. Downing, L. Hesselink, J. Ralston and R. Macfarlane, *Science*, 1996, **273**, 1185–1189.
9 B. Zhu, S. Zhang, S. Zhou, N. Jiang and J. Qiu, *Opt. Lett.*, 2007, **32**, 653–665.
10 D. Chen, Y. Yu, P. Huang, F. Weng and H. Lin, *Appl. Phys. Lett.*, 2009, **94**, 041909.
11 X. Li, H. Guo, Y. Wei, Y. Guo, H. Lu, H. Minoh and J. Jeong, *J. Lumin.*, 2014, **152**, 168–171.
12 H. Ping, D. Chen, Y. Yu and Y. Wang, *J. Alloys Compd.*, 2010, **490**, 74–77.

13 Y. Wei, X. Chi, X. Liu, R. Wei and H. Guo, *J. Am. Ceram. Soc.*, 2013, **96**, 2073–2076.
14 F. Liu, E. Ma, D. Chen, Y. Yu and Y. Wang, *J. Phys. Chem. B*, 2006, **110**, 20843–22086.
15 G. Bai, L. Tao, Y. Wang and Y. H. Tsang, *Integr. Ferroelectr.*, 2013, **142**, 31–36.
16 L. Huang, T. Yamashita, R. Jose, Y. Arai, T. Suzuki and Y. Ohishi, *Appl. Phys. Lett.*, 2007, **90**, 131116.
17 F. Xin, S. Zhao, L. Huang, D. Deng, G. Jia, H. Wang and S. Xu, *Mater. Lett.*, 2012, **78**, 75–77.
18 J. Cao, X. Li, Z. Wang, Y. Wei, L. Chen and H. Guo, *Sens. Actuators, B*, 2016, **224**, 507–513.
19 S. Ye, B. Zhu, J. Chen, J. Luo and J. Qiu, *Appl. Phys. Lett.*, 2008, **92**, 141112.
20 D. Chen, Y. Zhou, Z. Wan and H. Yu, *Phys. Chem. Chem. Phys.*, 2015, **17**, 7100–7103.
21 X. Li, J. Cao, Y. Wei, Z. Yang and H. Guo, *J. Am. Ceram. Soc.*, 2015, **98**, 3824–3830.
22 X. Li, J. Cao, F. Hu, R. Wei and H. Guo, *RSC Adv.*, 2017, **7**, 35147–35153.
23 Y. Hao, S. Lv, Z. Ma and J. Qiu, *RSC Adv.*, 2018, **8**, 12165–12172.
24 S. Jiang, P. Zeng, L. Liao, S. Tian, H. Guo, Y. Chen, C. Duan and M. Yin, *J. Alloys Compd.*, 2014, **617**, 538–541.
25 Y. L. Wei, X. M. Li and H. Guo, *Opt. Mater. Express*, 2014, **4**, 1367–1372.
26 S. Jiang, P. Zeng, L. Q. Liao, S. Tian, *et al.*, *J. Alloys Compd.*, 2014, **617**, 538–541.
27 H. Guo, N. Dong, M. Yin, W. Zhang, L. Lou and S. Xia, *J. Phys. Chem. B*, 2004, **108**, 19205–19209.
28 S. Zheng, W. Chen, D. Tan, J. Zhou, Q. Guo, W. Jiang, C. Xu and X. Liu, *Nanoscale*, 2014, **6**, 5675–5679.